Kobe University Repository : Kernel

PDF issue: 2025-12-05

Metal Oxide Coated Porous Silicon Electrode Fabricated by Anodized Liquid Phase Depositions

Mizuhata, Minoru
Katayama, Akihito
Maki, Hideshi

(Citation)
ECS Transactions,61(9):9-20

(Issue Date)
2014

(Resource Type)
journal article

(Version)
Version of Record

(Rights)
© 2014 ECS - The Electrochemical Society

(URL)
https://hdl.handle.net/20.500.14094/90005898

ECS Transactions, 61 (9) 9-20 (2014)
10.1149/06109.0009ecst ©The Electrochemical Society

Metal Oxide Coated Porous Silicon Electrode Fabricated by Anodized Liquid Phase Depositions

Minoru Mizuhata, Akihito Katayama, and Hideshi Maki

Department of Chemical Science and Engineering, Graduate School of Engineering, Kobe University, 1-1 Rokkodai-cho, Nada, Kobe 657-8501, Japan

The titanium oxide/PSi nanocomposite was fablicated by liquid phase deposition (LPD) method with applying anodic potential. Results of SEM-EDX measurement showed that TiO_2 deposited into the fine pore (ca. 7.4 nm) only when oxidized PSi surface was used as F^- scavenger or PSi was anodized under the existence of titanium ions. TiO_2/PSi nanocomposite was fabricated by anodization of PSi in H_2TiF_6 electrolyte under constant potential. As the amount of Ti maximized at 300 mV vs. Ag/AgCl, deposition process can be controlled by applied potential in this method. The charge/discharge capacities were measured for fabricated TiO_2/PSi as lithium-ion battery anode. The improvement of the capacity was derived from the increase in PSi wettability by TiO_2 deposition and activation of silicon in fine structure. In addition, TiO_2/PSi fabricated by anodization kept higher capacity without rapid degradation, because of free from SiO_2.

Introduction

Porous silicon, PSi, is fablicated by silicon anodization in etching solution(1), stain etching(2,3), and metal-assisted chemical etching(4,5). In addition, PSi can be also fablicated by a silicon wafer anodization in HF aqueous solution. PSi formation via anodization is controllable by change of the type and concentration of dopant in silicon wafer, HF_2^- concentration in etching solution and current density, and various pores can be formed. We attempted to deposit TiO_2 on PSi, which was formed by the LPD method which is effective for deposition of TiO_2 on PSi substrate having submicron ordered pores. SiO_2 generated by thermal oxidization of PSi substrate and silicon surface at anodic potential can be the candidates for F^- scavengers when attempting to deposit on TiO_2 on PSi by the LPD method. Therefore anodization of PSi in the LPD reaction solution is expected to be an easy process for fabrication of TiO_2/PSi nanocomposite. In this study, TiO_2/PSi nanocomposites were fabricated with the use of boric acid, oxidized PSi surface or silicon surface at anodic potential as an F^- scavenger.

TiO_2/PSi nanocomposites which were prepared by the LPD method are quite useful for lithium ion battery (LIB) anodes. Titanium oxide absorbs lithium ion as following reaction;

$$TiO_2 + \chi Li^+ + \chi e^- \leftrightarrow Li_\chi TiO_2 \qquad (1)$$

When TiO_2 electrode is used as LIB anode, the theoretical capacity is 170 $mAh \cdot g^{-1}$ and operating voltage is 1.75 V vs. Li^+/Li(6,7). Therefore, it can be estimated that TiO_2

Downloaded on 2015-04-30 to IP 133.30.98.14 address. Redistribution subject to ECS terms of use (see ecsdl.org/site/terms_use) unless CC License in place (see abstract).

electrode is inferior as compared with graphite (372 mAh·g^{-1}) from the aspect of capacity and energy density. However TiO_2 can absorb lithium with small volume change, thus TiO_2 can be the prominent anode material with the object to cycle property and safety. We attempted to deposit TiO_2 on Porous silicon (PSi) which has low resistivity (3.0-4.0 mΩ·cm) by the LPD method and fabricate TiO_2/PSi nanocomposite. Nanocomposites were fabricated by the LPD method with various F^- scavengers, and some of them held fine pores derived from PSi substrate and TiO_2 covered a part of PSi surface

.

Silicon substrate also can be active material for LIB anode when fabricated TiO_2/PSi nanocomposites were use as electrode.

$$Si + 4.4Li^+ + 4.4e^- \leftrightarrow Li_{4.4}Si \qquad (2)$$

It is well known that one silicon atom can absorb 4.4 lithium ions when silicon is used as LIB anode material, and the theoretical capacity of silicon is very large (ca. 4200 mAh·g^{-1}). In addition, the operating voltage of silicon is 0.0-0.4 V vs. Li^+/Li(8-10), which is relatively close to that of a lithium electrode, thus high energy density is expected. Besides, it is expected that the usage of PSi instead of silicon wafer enables electrode to perform high-speed charge/discharge and high-capacity charge which are derived from the large surface area. On the other hand, there is a disadvantage, that is, PSi causes high hydrophobicity because of its terminal group and lotus effect derived from fine structure(11). This indicates that silicon in porous layer does not work as an active material, and first charge capacity may decrease. The deposition of TiO_2 on the surface of PSi pore is effective method to solve the issue. Since TiO_2 is lithium storage material as well as superhydrophilic material, it is expected that effective surface area of PSi for electrode increase by deposition of TiO_2. In this study, TiO_2/PSi nanocomposites were used as LIB anode. The half-cell electrochemical measurements were performed with beaker cell.

Experimental

Fabrication of porous silicon(PSi)

Highly boron doped P-type single crystal (100) silicon wafer (Shin-Etsu Astech Co., Ltd.) was used as the working electrode. The thickness of silicon wafer was 625.0 ± 25.0 μm, and the resistivity of that was 3.00 - 4.00 mΩ·cm. Silicon wafer was cut into the size of 2 × 2 cm^2 with a diamond cutter. These were dipped in acetone and cleaned ultrasonically for 15 min to degrease, and taken out from acetone and dried at room temperature. The electrolysis cell made from Teflon® was prepared, and silicon wafer working electrode and platinum mesh counter electrode were fixed at the electrolysis cell. After 5 min of introduction of 5 wt% HF aqueous solution, 5 wt% HF aqueous solution was removed and HF/H_2O/EtOH mixed solution was introduced. The cell filled with the electrolyte was moved to dark room at room temperature, and the anodic oxidization of silicon electrode was carried out under galvanostatic condition (60 mA·cm^{-2}) for 10 min. The electrolyte was removed after the anodic oxidization. The silicon electrode was rinsed with deionized distilled water and methanol, and dried in Ar atmosphere at room temperature. The characterization of PSi was carried out by FE-SEM and the determination of the surface area and the pore size distributions with N_2-isotherm analysis.

Downloaded on 2015-04-30 to IP 133.30.98.14 address. Redistribution subject to ECS terms of use (see ecsdl.org/site/terms_use) unless CC License in place (see abstract).

Deposition of TiO_2 on silicon wafer or PSi by the LPD reaction with anodized Si as F^- scavenger

Silicon wafer or PSi working electrode, platinum mesh counter electrode, Ag/AgCl reference electrode and salt bridge were fixed in a three-electrode electrolysis cell. H_2TiF_6/H_2O/EtOH mixed solution was used as an electrolyte. Silicon working electrode was anodized in the electrolyte at constant potential (0-550 mV vs. Ag/AgCl). The reaction was performed for 30 min at room temperature. After anodization the working electrode was removed from solution and rinsed with deionized distilled water and methanol. The sample was dried in Ar atmosphere at room temperature. The characterization of TiO_2 thin film on silicon wafer was carried out by FE-SEM, XRD, FT-IR. The surface area was measured by multipoint BET method and the deposition amount of titanium was quantified by ICP-AES.

Electrochemical properties evaluation as an anode of lithium-ion battery

Lithium ribbon (Aldrich chemistry) stored in hexane was cut into 1×2 cm^2 rectangle, which was adequately rinsed with 1.0 $mol \cdot dm^{-3}$ $LiClO_4$-EC/DEC electrolyte and used as Li electrode. As-prepared PSi was thermally oxidized at 300 ºC for 4 min in air(12) by muffle furnace (KOYO Thermo Systems Co., Ltd). This oxidized PSi (SiO_2/PSi) was used as the electrode for reference measurement. The cyclic voltammetry measurements were performed to confirm the potential response between electrode and lithium ions by CompactStat-CompactStatPlus (Ivium technologies). The measurement was performed in the region of 0-3.0 V vs. Li^+/Li at 0.5 $mV \cdot s^{-1}$ sweep rate. The evaluation of charge/discharge capacity of each sample was performed. Charge/discharge was performed at 500 μA for each sample, and cut-off voltage was set to 0.01-3.50 V vs. Li^+/Li. Charge/discharge was repeated at most 15 times. The sample was arbitrarily taken out on the course of charge/discharge, rinsed with methanol (Nacalai tesque Inc.) and dried in Ar atmosphere. The sample was evaluated by other instruments. The morphology and the oxidation state on the surface of the fabricated TiO_2/PSi caused by charge/discharge were observed by FE-SEM and XPS, respectively.

Results and discussion

Fabrication of TiO_2/PSi nanocomposites by the LPD method

The silicon wafers were successfully anodized in HF/H_2O/EtOH mixed solution under a constant current which was 60 $mA \cdot cm^{-2}$ for 10 min. The depth of pore was about 27.7 μm, and the pore size distributions suggested that the electrochemically dissolved sample was uniform porous material which had fine pores with about 7.3 nm diameter. The surface area of PSi was 0.864 m^2 from the result of multipoint BET method. It was obvious that the surface structure of the sample has been complicated by etching process. PSi was immersed in $(NH_4)_2TiF_6/H_3BO_3$ or H_2TiF_6/H_3BO_3 mixed solution in which boric acid was used as F^- scavenger, and the LPD reaction was continued for 1 or 6 h. Fig. 1 shows SEM images and SEM-EDX line mappings for titanium of these samples. Top surface image showed that the mesopores derived from PSi substrate disappeared in the sample immersed in $(NH_4)_2TiF_6/H_3BO_3$ mixed reaction solution for 6 h. Furthermore, titanium was located on top of the porous layer as observed cross section SEM-EDS

Downloaded on 2015-04-30 to IP 133.30.98.14 address. Redistribution subject to ECS terms of use (see ecsdl.org/site/terms_use) unless CC License in place (see abstract).

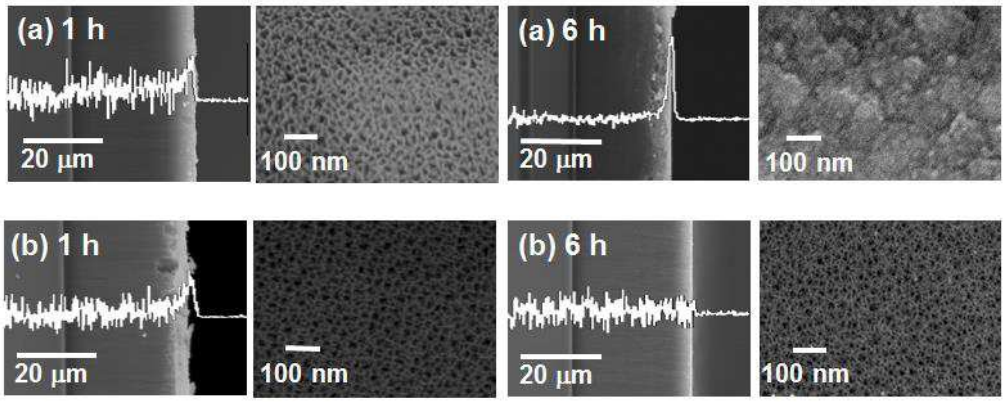

Fig. 1 SEM images and titanium line profiles after the LPD reaction where as-prepared PSi were used as substrates. (a):$(NH_4)_2TiF_6$-H_3BO_3 mixed reaction solution, (b): H_2TiF_6-H_3BO_3 mixed reaction solution, LPD reaction time: 1-6 h

measurement about the same sample. Thus, it can be estimated that the reason for disappearance of mesopores was the covering of substrate by deposited titanium oxide. In addition, it was observed that this titanium oxide deposited only out of the porous layer, and did not deposit in the pores. This phenomenon was caused by the poor wettability of PSi which disturbed reaction solution to intrude into porous layer(11). The deposition of titanium oxide was not observed from the PSi immersed in H_2TiF_6/H_3BO_3 mixed reaction solution. The pH of H_2TiF_6/H_3BO_3 mixed reaction solution was lower than that of $(NH_4)_2TiF_6/H_3BO_3$ mixed reaction solution and the increase in activity of F^- ions disturbed the hydrolysis reaction for the LPD method.

In order to improve the wettability of PSi surface or form SiO_2 layer used as F^- scavenger, as-prepared PSi was thermally oxidized(12). Fig. 2 shows SEM images and

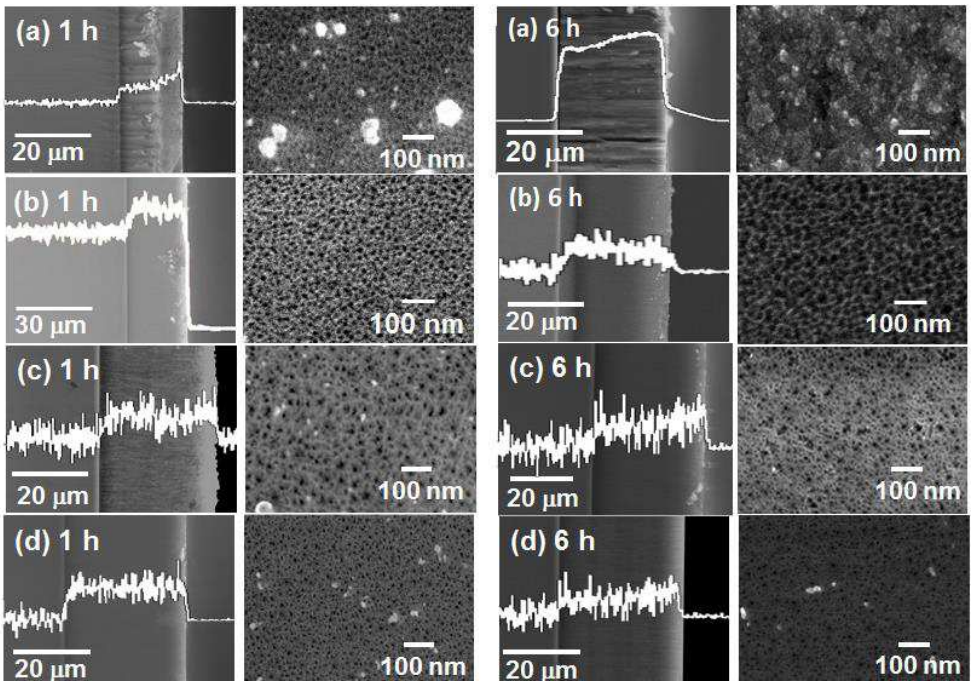

Fig. 2 SEM images and titanium line profiles after the LPD reaction where oxidized PSi were used as substrates. (a): $(NH_4)_2TiF_6$-H_3BO_3 mixed reaction solution, (b): $(NH_4)_2TiF_6$ reaction solution, (c): H_2TiF_6 reaction solution, (d): H_2TiF_6-H_3BO_3 mixed reaction solution, LPD reaction time: 1-6 h

Downloaded on 2015-04-30 to IP 133.30.98.14 address. Redistribution subject to ECS terms of use (see ecsdl.org/site/terms_use) unless CC License in place (see abstract).

SEM-EDS line profile for titanium of samples. SEM-EDS measurements for all samples indicated that titanium oxide was deposited in porous layer. These results were extremely different from those of non-oxidized PSi substrates. It was supposed that the difference was derived from the existence of silicon terminal groups (Si-H). The surface with Si-H group is known to work as a water shedding surface. In addition it is reported that Si-H group prevents fluorine to etch the silicon(11,13). Therefore, the PSi oxidization process at high temperature changed Si-H group to silanol group, which was active as F^- scavenger and made it possible for reaction solution to intrude into porous layer. When thermally oxidized PSi substrate was immersed in $(NH_4)_2TiF_6/H_3BO_3$ mixed reaction solution, titanium oxide filled the pores and deposited out of the porous layer (Fig. 2(a)). This was because titanium oxide core was generated by hydrolysis in bulk liquid with high speed due to high pH and boric acid. On the other hand, SEM observation suggested that PSi substrate structure was held even after the LPD reaction and titanium oxide was deposited on the wall surface in other systems. Since SiO_2 on the PSi surface was used as F^- scavenger in $(NH_4)_2TiF_6$ reaction solution and H_2TiF_6 reaction solution, the mean free pass of titanium oxide core generated by hydrolysis was quite short, thus on-site deposition of titanium oxide was performed. The XPS measurements were also supported these phemonena.

Therefore we also evaluated the novel nanocomposite fabrication process by the anodizations of the silicon wafer and PSi with the LPD reaction. The anisotropic etching will be preferred for the fabrication of the fine structured nanocomposites. Hence, we attempted to anodize silicon or PSi at the potential which caused nano-PSi formation or anisotropic etching (0-500 mV vs. Ag/AgCl) and fabricate nanocomposites. Before the formation of TiO_2/PSi nanocomposite, silicon wafer was used as an electrode and titanium oxide deposition on silicon wafer was attempted by anodization at 100-500 mV vs. Ag/AgCl. Fig. 3 shows the XPS spectra in range of Ti 2p about silicon wafer anodized at 100-500 mV vs. Ag/AgCl for 30 min in H_2TiF_6/H_2O/EtOH mixed solution. The peaks derived from titanium were observed from almost all samples, and especially the peaks of anodized sample at 300 or 400 mV vs. Ag/AgCl were shifted to low binding energy side (ca. 459.7 eV). It was suggested that titanium becomes chemically bonded to silicon substrate after considering the very flat substrate surface, washing process and XPS peak shift. Therefore it was indicated that the LPD reaction with the use of silicon at anodic potential was expected to be the novel candidate for nanocomposite fabrication

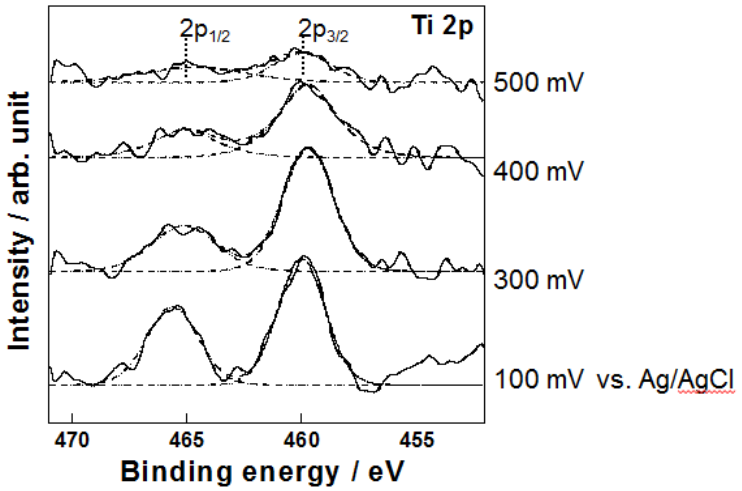

Fig. 3 XPS spectra for Ti 2p of silicon wafer anodized in H_2TiF_6/H_2O/EtOH mixed solution, LPD reaction time: 30 min

Downloaded on 2015-04-30 to IP 133.30.98.14 address. Redistribution subject to ECS terms of use (see ecsdl.org/site/terms_use) unless CC License in place (see abstract).

process. Fig. 4 shows SEM image and SEM-EDS line mapping for titanium of PSi anodized at 400 mV vs. Ag/AgCl for 30 min in H_2TiF_6/H_2O/EtOH mixed solution. The top surface observation confirmed that the fine pores with about 10 nm diameter were remained even after anodization. In addition, the SEM-EDS mapping indicates that the titanium oxide deposited in the porous layer. Therefore it was suggested that the on-site deposition of titanium oxide was successfully fabricated by the LPD method with the silicon at anodic potential as F^- scavenger. The pore size distributions of PSi anodized at various potential were measured with N_2-desorption isotherm. The pore diameter increased with an increasing of the applied potential, and the pore diameter of the nanocomposites fabricated by anodization of PSi for 30 min at 200-500 mV vs. Ag/AgCl were about 9.5 nm, thus, it is obvious that the pore wall was etched during the LPD reaction. Fig. 5 shows the FT-IR results of PSi anodized at constant potentials for 30 min in H_2TiF_6/H_2O/EtOH mixed solution. Three absorption bands at about 2100 cm^{-1} which were observed for all samples can be assigned to SiH_3 (2137 cm^{-1}), SiH_2 (2113 cm^{-1}) and

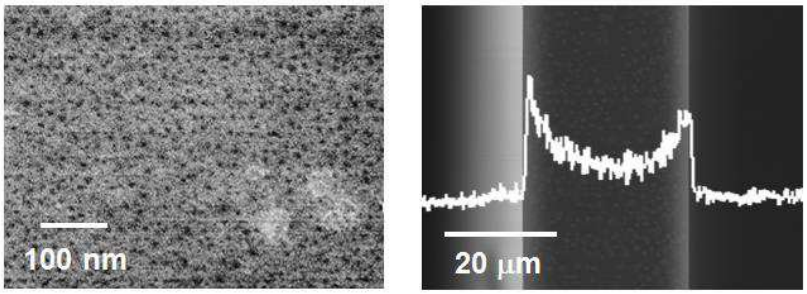

Fig. 4 SEM images and titanium line profile of TiO_2/PSi fabricated by anodization, applied potential: 400 mV vs. Ag/AgCl, LPD reaction time: 30 min

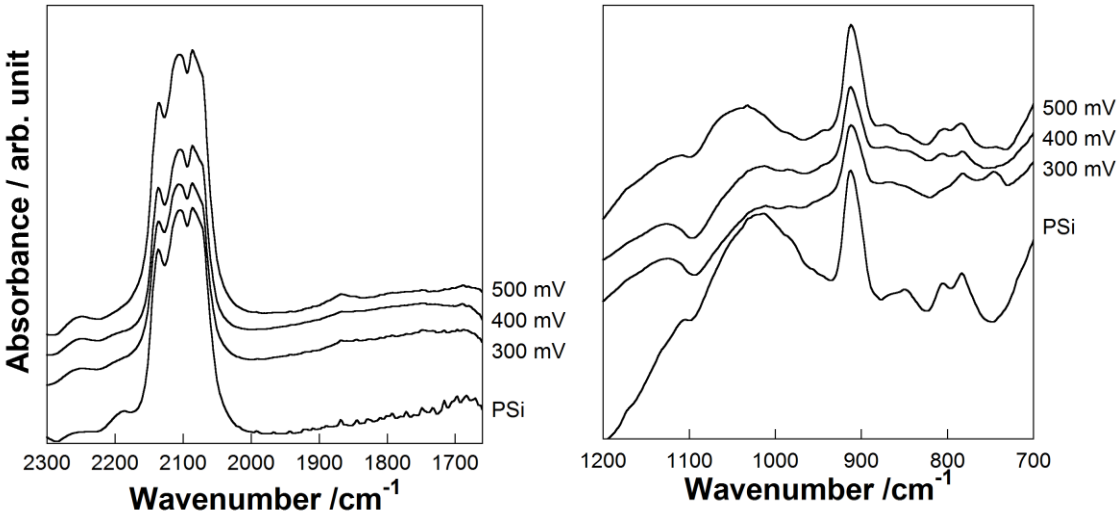

Fig. 5 FT-IR spectra of TiO_2/PSi fabricated by anodization, LPD reaction time: 30 min

SiH (2086 cm^{-1}) stretching mode, and the absorption band at about 908 cm^{-1} can be assigned to SiH_2 bending mode(14-16). On the other hand, the very weak ν_{SiO2} absorption band (1878 cm^{-1}) and the stretching vibration of Si-O-Ti^{4+} bond structure (940 cm^{-1}) were also observed in nanocomposites(17). These results indicate that the chemical bonds between titanium and the substrates were formed by anodization of PSi. Fig. 6(a) shows in the Ti 2p region of the XPS spectra of PSi which was anodized at 400 mV vs. Ag/AgCl for 30 min in H_2TiF_6/H_2O/EtOH mixed solution. H_2TiF_6 on silicon wafer was used as a reference sample for titanium peak shift. The peak at 460.0 eV is Ti $2p_{3/2}$ in

Downloaded on 2015-04-30 to IP 133.30.98.14 address. Redistribution subject to ECS terms of use (see ecsdl.org/site/terms_use) unless CC License in place (see abstract).

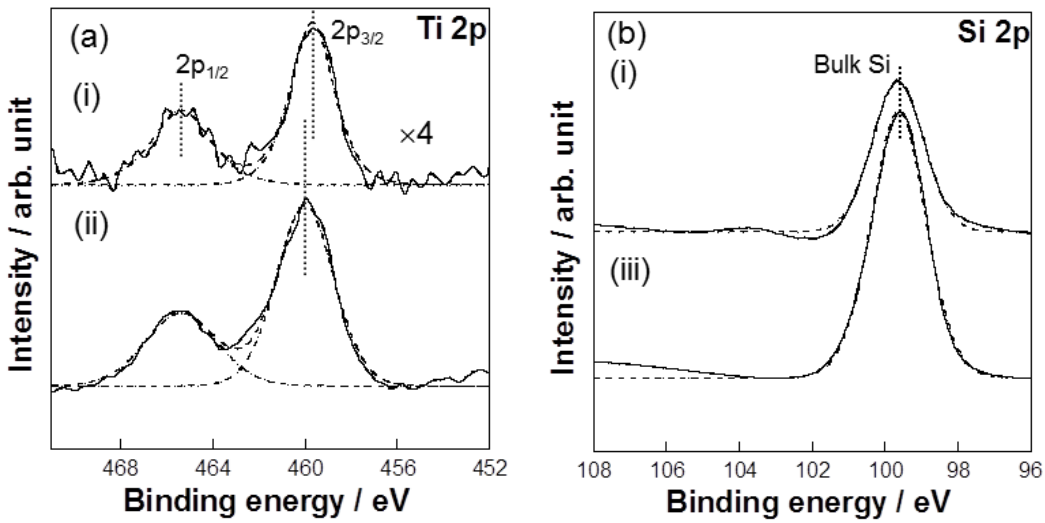

Fig. 6 XPS spectra for (a)Ti 2p and (b) Si 2p.(i): TiO_2/PSi fabricated by anodization, applied potential: 400 mV vs. Ag/AgCl, LPD reaction time: 30 min, (ii): silicon wafer on which H_2TiF_6 was dipped and dried, and (iii) as-prepared PSi.

reference sample, and the peak at 459.7 eV can be assigned the nanocomposite fabricated by the anodization in H_2TiF_6/H_2O/EtOH mixed solution. The peak top position shifted to the lower binding energy by the anodization. The removal of F^- ions and coordination of O^{2-} ions were occurred in these systems, that is, the LPD reaction was brought about. Fig. 6(b) shows XPS in the Si 2p region of the XPS spectra of the same sample and as-prepared PSi as a reference sample. While the peak which was derived from SiO_2 at 103.3 eV was observed from the nanocomposite fabricated via thermal oxidization by XPS measurement, the same peak was hardly observed from nanocomposites fabricated via anodic oxidization. SiO_2 formed as an intermediate is supposed to be dissolved by F^- ions immediately. Finally the quantification of the deposition amount of titanium oxide was performed about nanocomposites fabricated by anodization of PSi at constant potential in H_2TiF_6/H_2O/EtOH mixed solution for 30 min, and the result is shown in Fig. 7. The amount of titanium shows the local maxima at applied potential 300 mV vs. Ag/AgCl. This behavior was similar to that of the systems in which SiO_2 on the surface

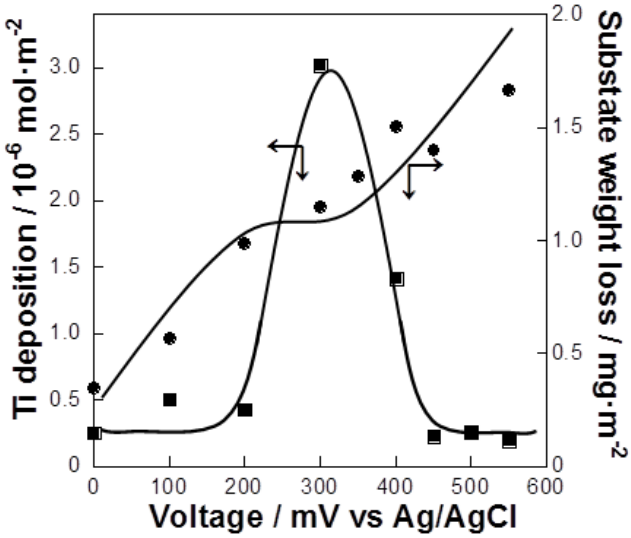

Fig. 7 Applied potential dependence of deposition amount of titanium and substrate weight loss. LPD reaction time: 30 min.

Downloaded on 2015-04-30 to IP 133.30.98.14 address. Redistribution subject to ECS terms of use (see ecsdl.org/site/terms_use) unless CC License in place (see abstract).

of PSi was used as F^- scavenger. Thus it was suggested that the behavior was derived from the competition reaction of the titanium fluoro-complex hydrolysis and anodized PSi dissolution. In other words, the poor F^- scavenger disturbed the LPD reaction at low potential, and the substrate dissolution disturbed the LPD reaction at high potential. This consideration was also supported by the observation of substrate weight loss as shown in Fig. 7. The nanocomposite fabricated by anodization at 300 mV vs. Ag/AgCl presented the largest amount of titanium deposition (3.02×10^{-6} mol·m^{-2}).

Electrochemical properties of TiO_2/PSi nanocomposites as an anode of Li-ion battery

Fig. 8 shows the result of the cyclic voltammograms(CV) of PSi, TiO_2/PSi(LPD-SiO_2) and TiO_2/PSi(LPD-anodized Si). At about 0.2 mA peak derived from the lithium insertion was observed in the region of 0.0-0.8 V vs. Li^+/Li from no-TiO_2 fabricated PSi.

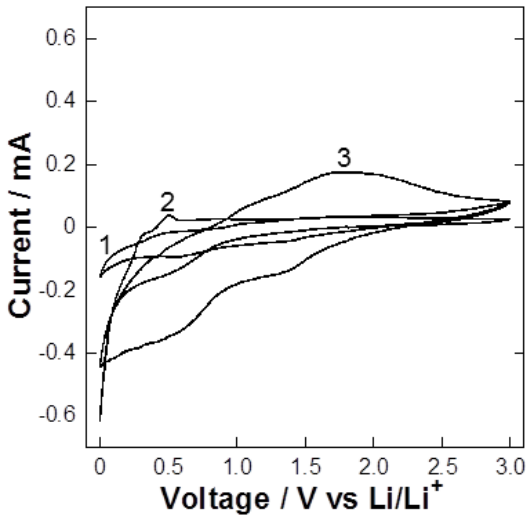

Fig. 8 Cyclic voltammograms of (1)PSi, (2)TiO_2/PSi(LPD-SiO_2) and (3)TiO_2/PSi(LPD-anodized Si) measured in the range of 0.0 -3.0 V vs. Li/Li^+ at 0.5 mV·s^{-1}.

On the other hand, the very broad peaks, which were thought to be derived from lithium insertion, were observed around the region of 0.5, 1.5 V vs. Li^+/Li from TiO_2/PSi nanocomposites. These CV curves indicated that fabricated TiO_2/PSi nanocomposites showed larger current derived from lithium insertion/extraction compared with non-TiO_2 fabricated PSi because of the improvement of the wettability and the increase in effective area for LIB anode. In addition, it was obviously observed that lithium was inserted in the range of 1.5 V vs. Li^+/Li and extracted in the range of 2.0 V vs. Li^+/Li as for TiO_2/PSi(LPD-anodized Si). These peaks at 1.5 V and 2.0 V vs. Li^+/Li were supposed to come from lithium insertion/extraction of TiO_2. Thus it was suggested that TiO_2 was under favorable environment to accept electron in TiO_2/PSi (LPD-anodized Si), in other words, most of TiO_2 existed not on SiO_2 insulator but on silicon semiconductor. While TiO_2/PSi(LPD-anodized Si) showed large current value in the region where lithium ions were extracted, PSi and TiO_2/PSi(LPD-SiO_2) showed small current value in the region.

The charge/discharge capacity measurements for each sample were performed on the voltage range of 0.01-3.50 V vs. Li/Li^+ at 500 μA. PSi showed 550 μAh of the first charging capacity by charge/discharge at 500 μA, and the capacity gradually decreased with charge/discharge cycles. Finally charging capacity of 15th cycle was 200 μAh.

Downloaded on 2015-04-30 to IP 133.30.98.14 address. Redistribution subject to ECS terms of use (see ecsdl.org/site/terms_use) unless CC License in place (see abstract).

TiO_2/PSi(LPD-SiO_2) and TiO_2/PSi (LPD-anodized Si) showed 850 μAh and 1700 μAh of the first charging capacity, respectively. These values were higher than that of PSi electrode, and it was suggested that the increase in the first capacity was derived from the improvement of the wettability by the deposition of TiO_2 and the activation of silicon in fine pore for LIB anode. This result shows good agreement with the CV measurements. However it was observed that rapid degradation of capacity occurred about TiO_2/PSi(LPD-SiO_2) after the first charging as can be seen in Fig. 9. This result also supported the CV measurements result in which lithium insertion current increased and extraction current did not increase. The reason can be presumed the deterioration of the substrate structure or the irreversible reaction of lithium in the first charging process. On

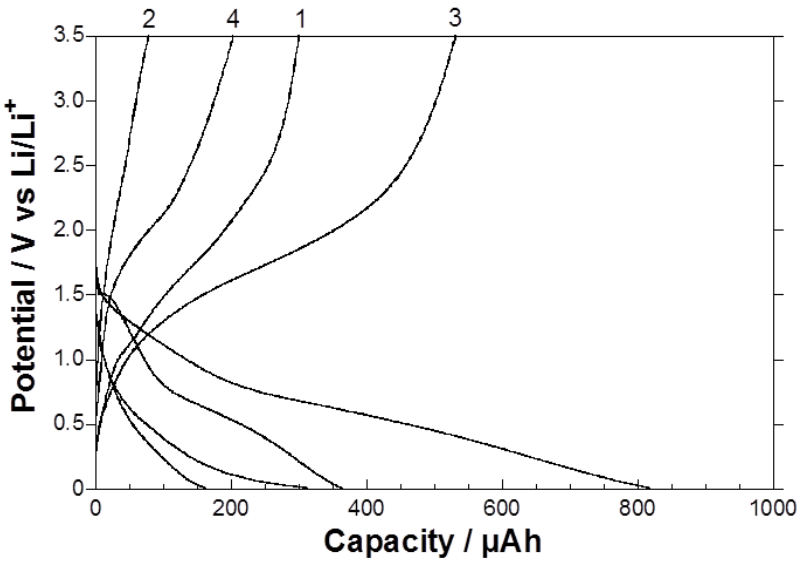

Fig. 9 Charge/discharge curves of each sample on the voltage range of 0.01-3.50 V vs. Li/Li^+ at 500 μA at the second cycles. (1) PSi, (2) TiO_2/PSi(LPD-SiO_2), (3) TiO_2/PSi(LPD-anodized Si), and (4) SiO_2/PSi.

the other hand, when TiO_2/PSi(LPD-anodized Si) was used as electrode, the rapid degradation of capacity was not observed, unlike TiO_2/PSi(LPD-SiO_2). The capacity gradually decreased with charge/discharge cycles, and the finally charging capacity of the 15th cycle was 200 μAh, and it was similar to that of no-TiO_2 fabricated PSi. Therefore it was suggested that one of the reason of the decrease in a capacity was detachment of TiO_2 caused by the charge/discharge as for TiO_2/PSi(LPD-anodized Si). This consideration was supported by the decrease in 1.0-1.5 V vs. Li^+/Li charging region where lithium thought to be inserted into TiO_2 with cycles. This hypothesis also supports that the silicon is well known to expand by the insertion of lithium(18). SiO_2/PSi showed 1280 μAh of the first charging capacity at 500 μA and rapid degradation of the capacity after the first charging as with TiO_2/PSi(LPD-SiO_2) as can be seen Fig. 9. This fact strongly supported that rapid capacity degradation of TiO_2/PSi(LPD-SiO_2) was related to the existence of SiO_2 in the electrode.

Fig. 10 shows the SEM images of PSi, TiO_2/PSi (LPD-SiO_2) and TiO_2/PSi (LPD-anodized Si) after 15th charge/discharge. The surface morphology of TiO_2/PSi (LPD-SiO_2) was quite different from other samples. The crack was not observed on porous layer even after the 15th charge/discharge in PSi and TiO_2/PSi(LPD-anodized Si), therefore it was supposed that the deterioration of structure was one of the factors which caused rapid capacity degradation of TiO_2/PSi(LPD-SiO_2). XPS measurement was

Downloaded on 2015-04-30 to IP 133.30.98.14 address. Redistribution subject to ECS terms of use (see ecsdl.org/site/terms_use) unless CC License in place (see abstract).

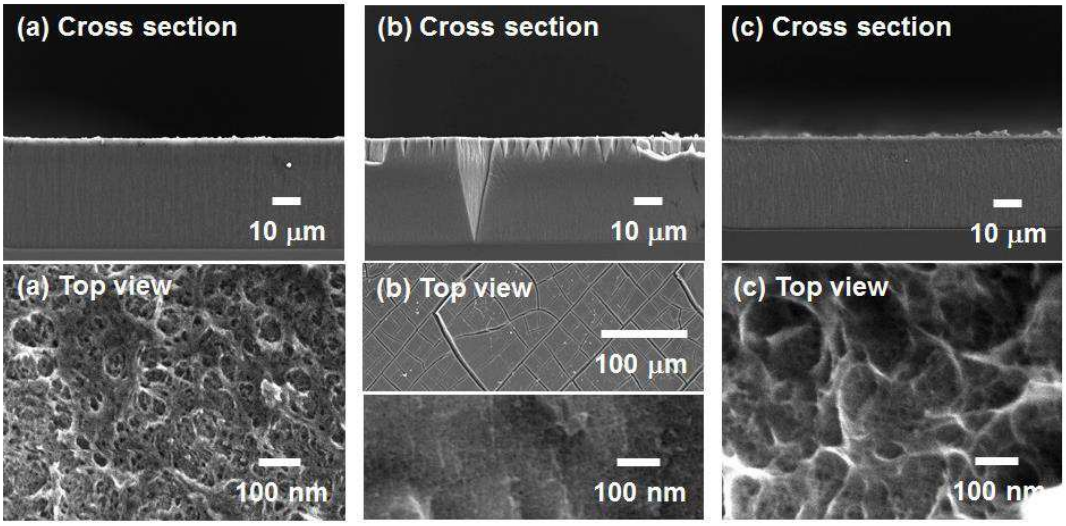

Fig. 10 SEM images after 15th charged/discharged (a): PSi, (b): TiO_2/PSi(LPD-SiO_2), (c): TiO_2/PSi(LPD-anodized Si) at 500 μA.

performed to investigate the oxidation states of PSi in the charge/discharge process. As-prepared, after the first charged and after the first charge /discharged PSi were used as samples. Fig. 11 shows the results of Si 2p and Li 1s measured by XPS. The storage of lithium can be confirmed from the full charged PSi because of the detection of the peak at 57.2 eV in the region of Li 1s. The peak at 104.4 eV was observed as well as the peak derived from Si^0 (99.6 eV) in the region of Si 2p from the same sample. However, the peak at 104.4 eV was unclear in spite of our expectation which this peak was related to silicon affected by carbon(19). Furthermore, the peak in Li 1s region disappeared after discharge, thus it was suggested that lithium was extracted from silicon again by discharging. Although we could not detect the peak derived from lithium-silicon alloy in Si 2p region, it was confirmed that ionized lithium existed in electrode because of comparison with the peak derived from lithium metal.

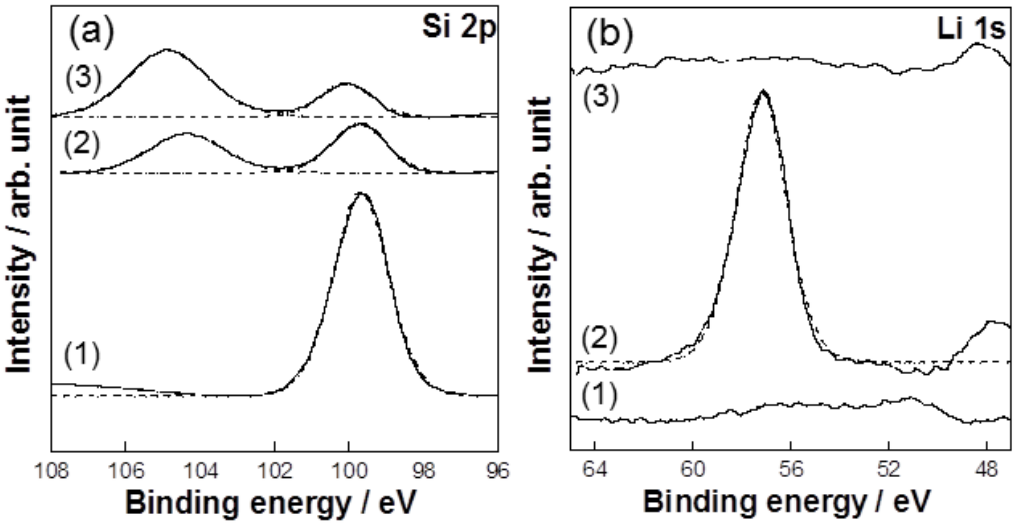

Fig. 11 XPS spectra for (a)Si 2p and (b) Li 1s of PSi on the process of charge/discharge. (1): As-prepared, (2): charged, and (3) discharged.

Fig. 12 shows the XPS spectra for TiO_2/PSi(LPD-SiO_2). It was observed that the new peaks emerged in the lower binding energy region of Ti 2p as for 300 μAh charged

Downloaded on 2015-04-30 to IP 133.30.98.14 address. Redistribution subject to ECS terms of use (see ecsdl.org/site/terms_use) unless CC License in place (see abstract).

TiO_2/PSi(LPD-SiO_2). This indicated that the part of tetravalent titanium in TiO_2 was reduced to trivalent titanium during charging process. Therefore, it was suggested that lithium was inserted into TiO_2, as expressed in reaction (1), until the potential reached to

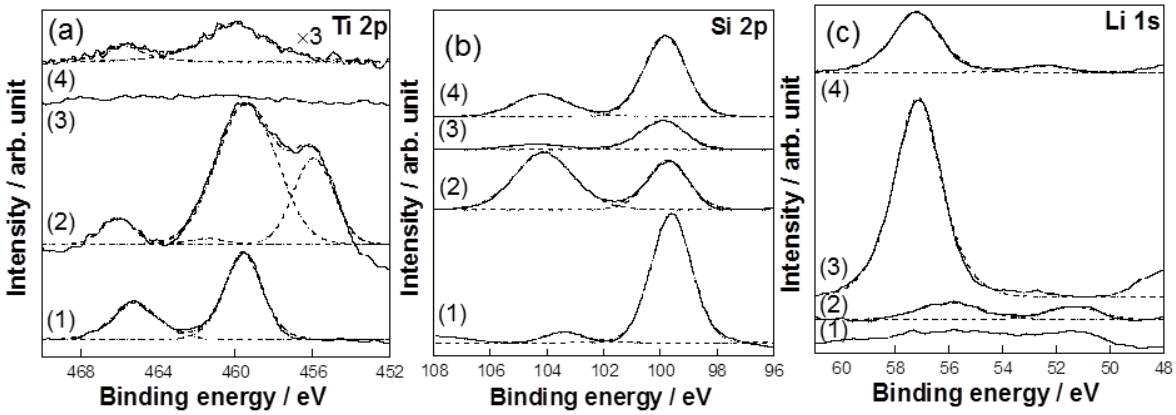

Fig. 12 XPS spectra for (a)Ti 2p, (b)Si 2p and (c)Li 1s of TiO_2/PSi(LPD-SiO_2) on the process of charge/discharge. (1): As-prepared, (2): 300 μAh charged, (3) full charged, and (4)discharged.

ca. 0.8 V vs. Li^+/Li in charge process. Since the trivalent titanium was oxidized to tetravalent titanium after discharge, TiO_2 is seemed to react with lithium reversibly. However the peak intensities derived from the titanium in the charged/discharged sample were lower than those in the as-prepared sample. It was suggested that TiO_2 in TiO_2/PSi was detached by the silicon substrate volume with the lithium insertion and extraction, thus the amount of TiO_2 decreased. In addition, the peak at 57.2 eV in Li 1S region was observed after the full charge. This indicates that lithium is inserted into TiO_2/PSi(LPD-SiO_2). However this peak remained even after discharge. This behavior is quite different from the result of the no-TiO_2 fabricated PSi as shown in Fig. 11, and it was suggested that lithium was not extracted from TiO_2/PSi(LPD-SiO_2) by discharging. The reason of this phenomenon was thought to be residual SiO_2 in TiO_2/PSi (LPD-SiO_2). Therefore lithium inserted into the electrode irreversibly reacted with SiO_2 as following reaction(20);

$$2SiO_2 + 4Li \rightarrow Si + Li_4SiO_4 \qquad (3)$$

SiO_2 remained in the nanocomposite fabrication process, and caused rapid degradation of capacity after first charge.

Conclusions

In this study, TiO_2/PSi composites were fabricated by the LPD method. The hydrolysis of metal fluoro-complex was promoted by various F- scavengers, i.e. boric acid and silicon dioxide which were generated by the thermal oxidization and the anodized silicon. On-site deposition of TiO_2 was especially observed from the composites fabricated by solid F^- scavengers like SiO_2 and anodized silicon. These samples held large surface area derived from PSi substrate. Thus it was suggested that novel LPD method without boric acid was effective for fabrication of TiO_2/PSi nanocomposites. Furthermore, the electrochemical properties for LIB anode of TiO_2/PSi nanocomposites fabricated by the LPD method were confirmed. The poor wettability of PSi was improved by the

Downloaded on 2015-04-30 to IP 133.30.98.14 address. Redistribution subject to ECS terms of use (see ecsdl.org/site/terms_use) unless CC License in place (see abstract).

deposition of TiO_2 on a surface of the nano-ordered fine structure in the PSi. When TiO_2/PSi nanocomposites were used as electrode, silicon in fine pore also worked as an active material and the capacity increased dramatically by the improvement of the wettability. However, in the case of the SiO_2 which was prepared by the conventional LPD method, the SiO_2 in the fabricated nanocomposite and the SiO_2 irreversible reaction with lithium brought about the rapid capacity degradation when used as LIB anode. Silicon surface at anodic potential was used as F^- scavenger in the novel LPD method, and it is the new TiO_2/PSi fabrication method which is free from SiO_2 insulator. TiO_2/PSi fabricated by the novel LPD method actually showed high capacity and reversible reaction, although the electrode exhibits capacity decrease typical of silicon based anodes.

This study is supported by JST-CREST of Japan.

References

1. F.A. Harraz, T. Tsuboi, J. Sasano, T. Sakka and Y. H. Ogata, *J. Electrochem. Soc*., **149**, C456-463 (2002)
2. D. R. Turner, *J. Electrochem. Soc*., **107**, 810-816 (1960)
3. M. E. Dudley and K. W. Kolasinski, *J. Electrochem. Solid-State Lett*., **12**, D22-D26 (2009)
4. Y. Qu, L. Liao, Y. Li, H. Zhang, Y. Huang, and X. Duan, *Nano Lett*., **9**, 4539-4543 (2009)
5. L. Lin, S. Guo, X. Sun, J. Feng, Y. Wang, *Nanoscale Res. Lett*., **5**, 1822-1828 (2010)
6. J. S. Chen, L. A. Archer and X. W. Lou, *J. Mater. Chem*., **21**, 9912-9924 (2011)
7. T. Djenizian, I. Hanzu and P. Knauth, *J. Mater. Chem*., **21**, 9925-9937 (2011)
8. K. Nishio, S. Tagawa, T. Fukushima, and H. Masuda, *Electrochem. Solid State Lett*., **15**, A41-A44 (2012)
9. E. V. Astrova, G. V. Fedulova, I. A. Smirnova, A. D. Remenyuk, T. L. Kulova, and A. M. Skundin, *Tech. Phys. Lett*., **37**, 731-734 (2011)
10. H. C. Shin, J. A. Corno, J. L. Gole, M. Liu, *J. Power Sources*, **139**, 314–320 (2005)
11. Y. Kato, S. Adachi, *Appl. Surf. Sci*., **258**, 5689-5697 (2012)
12. J. Riikonen, M. Salomäki, J. van Wonderen, M. Kemell, W. Xu, O. Korhonen, M. Ritala, F. MacMillan, J. Salonen, and V.P. Lehto, *Langmuir*, **28**, 10573-10583 (2012)
13. K. W. Kolasinski, *J. Phys. Chem. C*, **114**, 22098–22105 (2010)
14. T. Arigane, K. Yoshida, T. Wadayama, A. Hatta, *Surf. Sci*., **427-428**, 304-308 (1999)
15. E. J. Anglin, M. P. Schwartz, V. P. Ng, L. A. Perelman, and M. J. Sailor, *Langmuir*, **20**, 11264-11269 (2004)
16. N. H. Zoubir, M. Vergnat, T. Delatour, A. Burneau, Ph. de Donato, O. Barrès, *Thin Solid Films*, **255**, 228-230 (1995)
17. S. M. El-Sheikh, O. A. Fouad, Y. M. Z. Ahmed, *J. Non-Cryst. Solid*, **358**, 2816-2825 (2012)
18. H. Li, X. Huang, L. Chen, Z. Wu, and Y. Liang, *Electrochem. Solid-State Lett*., **2**, 547-549 (1999)
19. M. Lu, Y. Tian, X. Zheng, J. Gao, B. Huang, *Int. J. Electrochem. Sci*., **7**, 6180-6190 (2012)
20. B. Philippe, R. Dedryvère, J. Allouche, F. Lindgren, M. Gorgoi, H. Rensmo, D. Gonbeau, and K. Edström, *Chem. Mater*., **24**, 1107-1115 (2012)

Downloaded on 2015-04-30 to IP 133.30.98.14 address. Redistribution subject to ECS terms of use (see ecsdl.org/site/terms_use) unless CC License in place (see abstract).